Engineering Structures 289 (2023) 116248

Contents lists available at ScienceDirect

Engineering Structures

journal homepage: www.elsevier.com/locate/engstruct

Post-earthquake performance and damage evaluation of self-centering shear wall with replaceable devices

Shuijing Xiao [a,*], Longhe Xu [b,*], Peng Feng [a]

[a] Department of Civil Engineering, Tsinghua University, Beijing 100084, China
[b] School of Civil Engineering, Beijing Jiaotong University, Beijing 100044, China

ARTICLE INFO

Keywords:
Self-centering shear wall
Disc spring
Cyclic loading test
Post-earthquake performance
Damage evolution

ABSTRACT

Self-centering structures have been demonstrated to be an effective method by which to improve seismic resilience. Most related research is focused on the seismic performance of self-centering structures without initial damage, whereas the post-earthquake performance of structures, which is significant for their repair and operation, is less investigated. Based on this, this study aims to evaluate the post-earthquake behavior and explore the damage evolution of a novel self-centering shear wall with replaceable devices, including disc springs to apply restoring force and friction pads to dissipate energy. Cyclic loading tests were conducted on two intact self-centering shear walls to investigate their seismic performance in our previous studies, and limited damage was observed after the tests. Thus, in this study, cyclic loading was directly applied to the two damaged self-centering shear walls to obtain their post-earthquake performance. The results indicate that the damaged self-centering shear walls exhibited satisfactory seismic behavior; their bearing capacity was reduced at small drift ratios as compared to that of the intact specimens, whereas no decrease of their bearing capacity occurred even at a 3% drift ratio. Moreover, the damaged self-centering shear wall exhibited appreciable energy dissipation and self-centering capabilities, and the residual drift ratio was less than 0.5% at a 2.1% drift ratio. However, the damage at the bottom of the RC wall after the post-earthquake test was obvious, revealing that the novel self-centering RC shear wall would need to be repaired after several earthquakes. Therefore, two effective methods were further developed to improve the post-earthquake performance of the novel self-centering shear wall.

1. Introduction

Earthquakes are recognized as one of the most destructive hazards due to the resulting structural function interruption and enormous repair or reconstruction costs. Therefore, many methods have been proposed to improve the seismic performance of structures to prevent their collapse. With the development of society, new requirements for the recoverability function of a structure after an earthquake have been put forward. As a result, numerous studies have been carried out to improve the seismic resilience of structures. Self-centering technology is one of the most effective methods by which to achieve resilient structures that require little to no repair after earthquakes [1–7].

As an important anti-lateral force component in high-rise buildings, the reinforced concrete (RC) shear wall significantly affects the seismic performance of the entire structure. Therefore, many novel self-centering RC shear walls have been developed to improve their seismic resilience. The unbonded post-tensioned (PT) tendon is commonly and extensively used to provide the restoring force for self-centering hybrid RC walls [8–12]. Kurama et al. [13,14] evaluated the seismic behavior of a set of unbonded PT precast RC walls. The results indicated that the design parameters of the post-tensioning force, the initial stress, and the eccentricity of the PT tendon were the key factors that affected the seismic behavior of the wall. Sritharan et al. [15] developed an innovative seismic resistance system consisting of a precast wall and two end columns (PreWEC), in which the wall and end columns were anchored individually to the foundation using unbonded PT tendons. The PreWEC system was demonstrated to have a lateral load-carrying capacity similar to that of a comparable RC wall, while minimizing damage and exhibiting a good self-centering capability. It should be noted that previous research has mainly been focused on the development of a novel configuration of self-centering shear walls and the investigation of their hysteretic behavior [16–20], and the post-

* Corresponding authors.
E-mail addresses: sjxiao@bjtu.edu.cn (S. Xiao), lhxu@bjtu.edu.cn (L. Xu).

https://doi.org/10.1016/j.engstruct.2023.116248
Received 21 October 2022; Received in revised form 26 April 2023; Accepted 29 April 2023
Available online 17 May 2023

earthquake seismic performance of self-centering shear walls has been less reported. In fact, because aftershocks always follow a larger earthquake, the mechanical behavior of the self-centering shear wall after an earthquake is very important; whether a structure can operate directly or must be repaired after a major earthquake is a require consideration. Therefore, it is necessary to investigate the post-earthquake mechanical behavior of the self-centering shear wall to provide repair recommendations after earthquakes.

To achieve self-centering capability and prevent the concrete wall toes from damage, a new type of self-centering shear wall with replaceable devices was proposed and tested in the authors' previous research [21,22]. As shown in Fig. 1(a), two replaceable disc spring (DS) devices are symmetrically installed at the foot of the specimen to prevent concrete crushing, the restoring force is simultaneously provided by combination DSs, and more seismic energy can be dissipated by installing friction pads in the DS devices. The manufacture of the RC wall panel is the same as that of the conventional RC shear wall, and the DS device is connected to the wall with high-strength bolts. Thus, it is convenient to replace and repair it after an earthquake. Experimental results indicated that the self-centering shear wall exhibited good energy dissipation and self-centering capabilities (Fig. 1(c)), and its residual drift ratio (less than 0.5%) was well controlled. However, minor damage was observed at the bottom corners of the RC wall, and its influence on the post-earthquake mechanical behavior of the self-centering shear wall was not clear. Therefore, the damage evolution of two self-centering shear walls under the first cyclic loading condition was further investigated in this study. Then, without repair, cyclic loading was applied on the two pre-damaged self-centering shear walls again to determine their mechanical behavior after an earthquake. Based on this, two effective methods were developed to improve the post-earthquake performance of the self-centering shear wall.

2. Damage evolution of the novel self-centering shear wall

2.1. General information about the specimens

Two novel self-centering shear walls (denoted as W1 and W2, respectively) were designed and tested in this study. The length, thickness, and height of the RC wall panels for W1 and W2 were 1.0, 0.125, and 2.0 m, respectively. Two reserved holes were set at the two bottom corners to install the replaceable DS devices. The length, thickness, and height of the holes for W1 were 0.24, 0.125, and 0.3 m, respectively, and those for W2 were 0.24, 0.125, and 0.5 m, respectively. More importantly, the replaceable DS devices of W1 were only equipped with combined DSs, whereas those of W2 were equipped with combined DSs and friction pads; thus, more energy counld be dissipated by the friction of W2. For W2 in stage I, no torque was stressed to the friction bolts, namely the value of friction was zero. In stage II, only the vertical load of W1 was increased to verify the axial bearing capacity and consider the influence of the live load during repair construction of the novel self-centering shear wall after an earthquake. On the other hand, only the friction of W2 was changed to investigate the effect of the additional friction on the hysteresis behavior of the novel self-centering shear wall after an earthquake. More detailed parameters of the two novel self-centering shear walls have previously been introduced [21,22]. The loading protocol of the tests, which included two loading stages, is shown in Fig. 2. In stage I, the loading protocol of each specimen before yielding was force-controlled, that after yielding was displacement-controlled, and the maximum drift ratio of the specimen was 3%; this met the seismic requirements in GB50011 [23]. After the cyclic loading test in stage I, the specimens remained on the loading setup and the loading protocol in stage II (which was controlled by displacement) was then applied to investigate their post-earthquake performance, as shown in Fig. 2. Because the hysteresis behavior of the novel self-centering shear wall was relatively stable at larger drift ratios according to the test results in stage I, the displacement amplitude with three cycles was applied at lower drift ratios and that with two cycles was applied at higher drift ratios. It should be noted that, benefiting from the replaceable devices of the novel wall configuration, the plastic damage at the bottom corners of the specimen could be addressed so that the specimens could be retested to obtain their post-earthquake mechanical behavior.

2.2. Damage evaluation

The damage state of the test specimens at a 2.1% drift ratio during the cyclic loading test in stage I is shown in Fig. 3. The damage of the two novel shear walls occurred in the following manner. The concrete next to

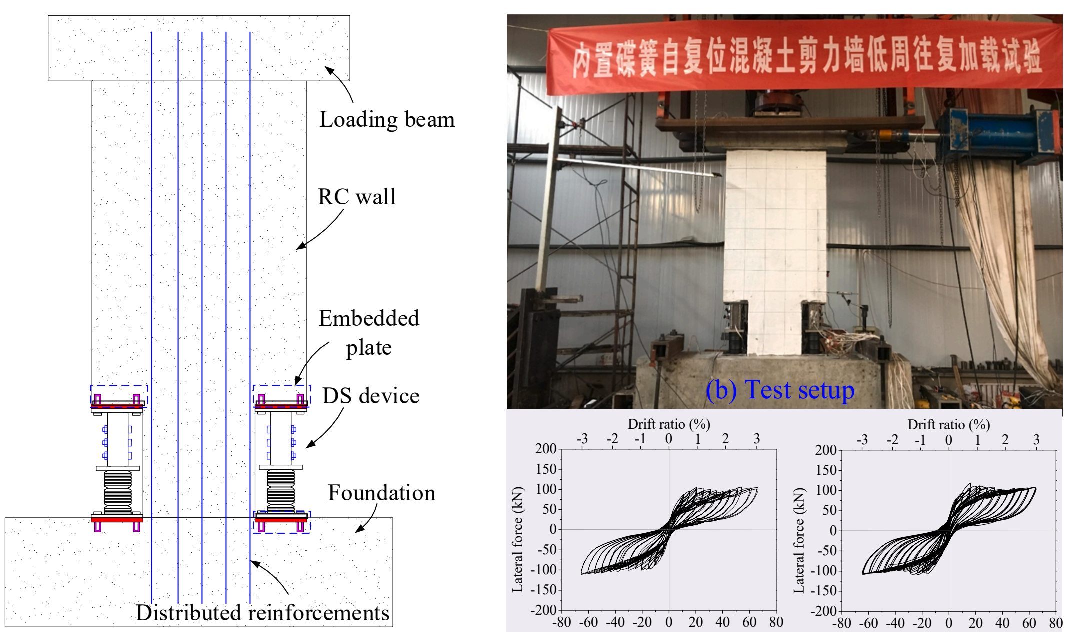

(a) Configuration (c) Hysteretic curves

Fig. 1. The novel self-centering shear wall with replaceable devices.

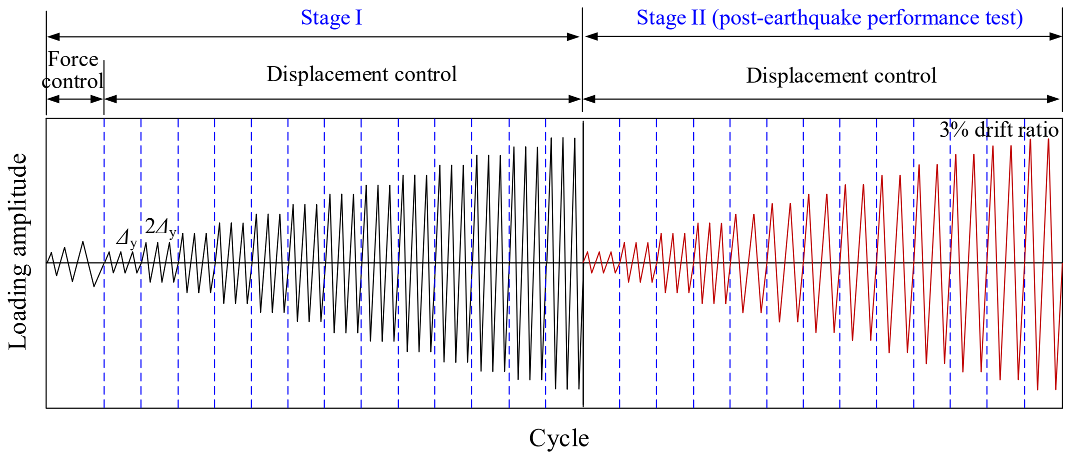

Fig. 2. The loading protocol of the tests.

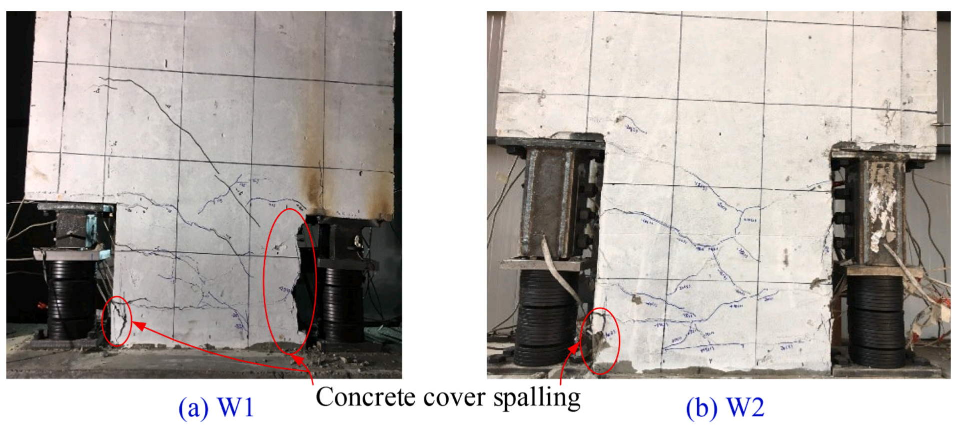

Fig. 3. The damage state of the test specimens at a 2.1% drift ratio.

the replaceable DS devices cracked horizontally at a height of 300 mm (W1) or 500 mm (W2), and the cracks expanded horizontally and diagonally with the increase of the lateral loading displacement. The longitudinal reinforcement of the middle wall panel next to the replaceable DS devices exhibited tensile yielding, and the local concrete cover of the wall panel next to the replaceable DS devices was crushed and spalled at a 2.1% drift ratio. However, the width of the cracks was less than 0.5 mm, and the cracks could be easily closed after unloading.

Although concrete cover spalling was observed after the strong earthquake, the steel bar was still not exposed. Therefore, the friction of the DS device had a minor effect on the damage evolution of the specimens, and obvious concrete spalling of both W1 and W2 was observed under strong earthquake conditions. However, their ultimate bearing capacity was only slightly affected and their residual drift ratio was greatly reduced [21,22]; thus, the specimens could still be tested.

To further evaluate the damage of the novel shear walls during the cyclic loading test in stage I, the strains of the concrete and reinforcements of the specimens were calculated. According to the strain time history of the concrete, the concrete strain basically increased with the increase of the loading displacement. More importantly, the strain gauges at the bottom of W1 and W2 were invalid when loading to a 3% drift ratio due to the wider cracks. Thus, the variation in concrete strain along the height of the test specimens at a 2.1% drift ratio was calculated, as shown in Fig. 4. Eight strain gauges were symmetrically placed

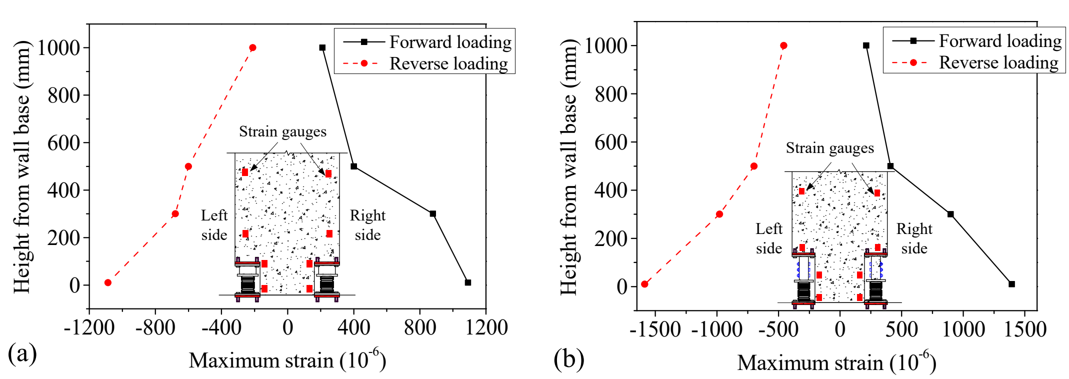

Fig. 4. The variation in concrete strain along the height of the test specimens at a 2.1% drift ratio: (a) W1, and (b) W2.

at two sides of the RC wall along the heights of 0, 300, 500, and 1000 mm, respectively. The concrete strain of both W1 and W2 gradually decreased with the increase of the height of the RC wall, and that at the bottom zone was much greater than that at the upper area, indicating more severe damage at the bottoms of both novel specimens. The maximum concrete compressive strain values of W1 and W2 at a 2.1% drift ratio were respectively 0.0011 (recorded by the strain gauge on the right side) and 0.0016 (recorded by the strain gauge on the left side), which were still less than the concrete peak strain of 0.002. Therefore, according to the concrete strain analysis, the damage of the novel self-centering shear walls under cyclic loading in stage I was not so significant.

The variation in the longitudinal reinforcement strain of the test specimens is shown in Fig. 5. Several strain gauges were placed at key positions of the longitudinal reinforcements. It can be seen that the strain of the steel bars in the boundary of the novel self-centering shear walls was relatively larger than that in the middle due to the larger deformation of the boundary part under cyclic loading. It can be seen that the maximum strains of the longitudinal reinforcements at two sides of the specimens during forward reverse loadings were not similar, especially for W1 (Fig. 5(a)). This is mainly because the damage occurred at one side of the wall specimen is more severe than the other side, as shown in Fig. 3, then the deformation of the longitudinal reinforcements at two sides was not completely symmetric. For the longitudinal reinforcement at the edge, the maximum strain of W1 and W2 was 0.0019 and 0.0014, respectively, which was less than the yield strain of the steel bar of 0.0021. Therefore, according to the strain analysis of the steel bars, the damage of the novel self-centering shear walls after one cyclic loading test was also not so significant.

The strain time history of the replaceable DS devices of the test specimens is presented in Fig. 6. The strain of the replaceable DS device gradually increased with the loading cycle, and the maximum strain values of the replaceable DS devices of W1 and W2 during the cyclic loading tests in stage I were 0.00097 and 0.00048, respectively. The maximum strain of the replaceable DS device of W2 was lower than that of W1 due to the higher friction of the combination DSs; nevertheless, the maximum strains of the replaceable DS devices of W1 and W2 were far less than the yield strain of steel. Therefore, the replaceable DS devices remained elastic during the seismic test in stage I, and they could stably provide restoring force and protect the RC wall of the novel self-centering shear wall system after an earthquake.

In summary, according to the strain analysis, the damage of the novel self-centering shear walls observed during the seismic test in stage I was theoretically acceptable; the walls could be rapidly repaired after an earthquake due to their satisfactory self-centering capability [21,22,24]. Because the damage was mainly concentrated on the RC wall panel, different parameters of the replaceable DS device had little impact on the failure of the self-centering shear wall. In general, because aftershocks always follow a major earthquake, the repair of the damaged structures cannot be carried out in time; thus, the post-earthquake performance of the novel shear wall is very important for emergency rescue work, and it can provide detailed suggestions for the repair of structures after earthquakes.

3. Seismic performance of the damaged self-centering shear wall

3.1. General information

The post-earthquake performance tests of the novel self-centering shear walls were conducted on a reaction frame at Baoheyuan Electronic Device Co., Ltd., Beijing. The test setup for the damaged specimens is shown in Fig. 7. The two specimens used during the post-earthquake test had initial damage at the bottom zone. The installation of the damaged test specimens was the same as that of the intact specimens [21,22]; each specimen was fixed by anchor beams, and out-of-plane braces were erected on both sides of the specimen to prevent significant out-of-plane deformation. After the cyclic loading test in stage I, the vertical and lateral loads of the specimens were removed. Then, during the cyclic loading test in stage II, a vertical load was reapplied at the top of the specimens by the jack and kept at constant values of 716.3 kN and 477.5 kN for W1 and W2, respectively. The cyclic lateral load was reapplied by the hydraulic actuator via displacement control (Fig. 2). Moreover, the high-strength bolts connecting the DS devices to the RC wall and foundation were re-tightened, and friction (the value was 34.3 kN) of the DS devices of W2 was applied before the post-earthquake tests.

3.2. Crack development

Fig. 8 presents the crack distribution of the test specimens at different drift ratios during the cyclic loading tests in stage II. Based on their initial damage at stage I, the damage of the two novel self-centering shear walls during the seismic tests became more severe when subjected to cyclic loading at stage II. The crack widths of both specimens increased with the increase of the drift ratio. However, the distribution zones of the cracks of the two novel specimens at stage II were similar to those that at stage I, as shown in Figs. 2 and 8; this indicates that the severe damage of the specimens was mainly concentrated at the bottom of the RC wall and the other parts of the specimens remained intact. For W1, obvious spalling of the concrete cover was observed at the bottom of both sides of the RC wall when the drift ratio reached 1%. Subsequently, as the load displacement increased, the concrete cover spalling extended from the edges of the wall panel to the middle, and longitudinal and distributed reinforcements were exposed at a 2% drift ratio. When the drift ratio reached 3%, the buckling of the longitudinal reinforcement at the boundary occurred, and the damage of the specimen was significant; at this point, the post-earthquake test was stopped. Similarly, the damage evolution of W2 was the same as that of W1; severe concrete

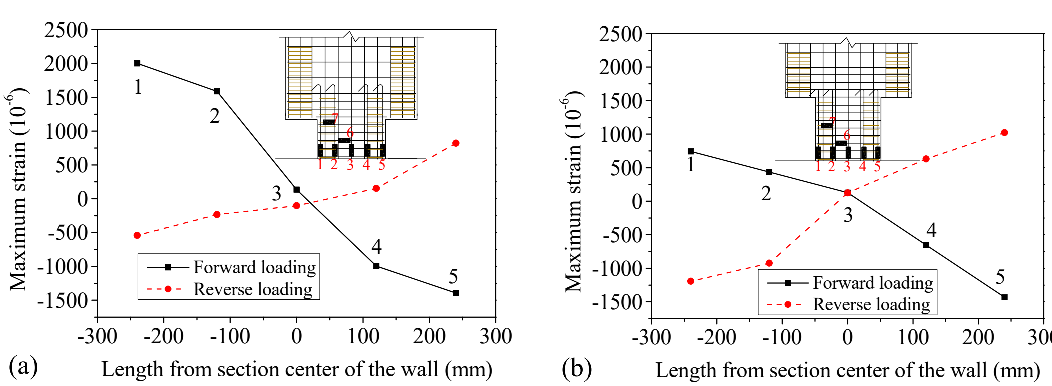

Fig. 5. The variation in the strain of the longitudinal reinforcements of the test specimens: (a) W1 and (b) W2.

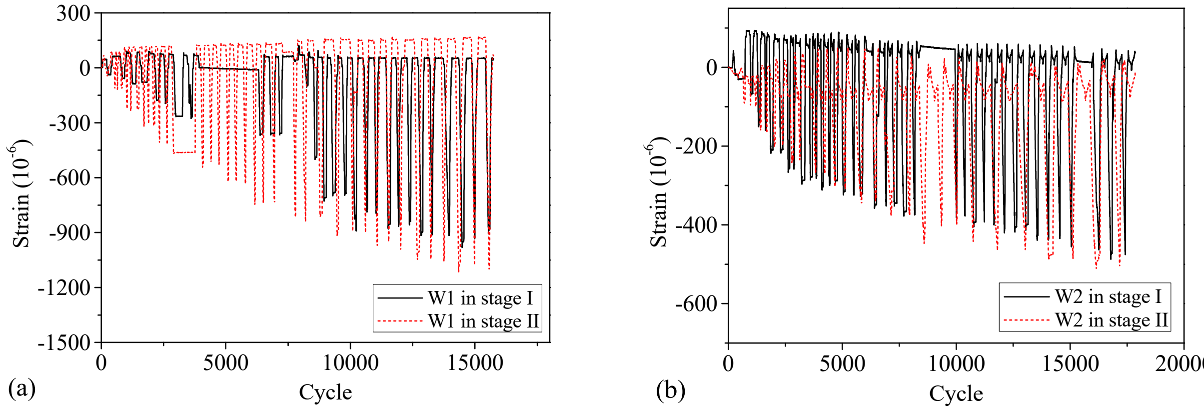

Fig. 6. The strain time history of the DS devices of the test specimens: (a) W1 and (b) W2.

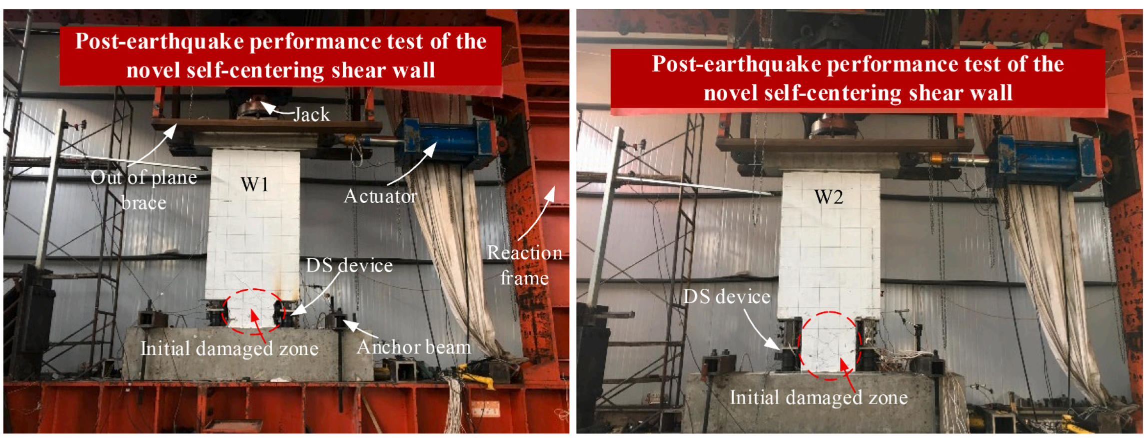

Fig. 7. The test setup for the damaged specimens.

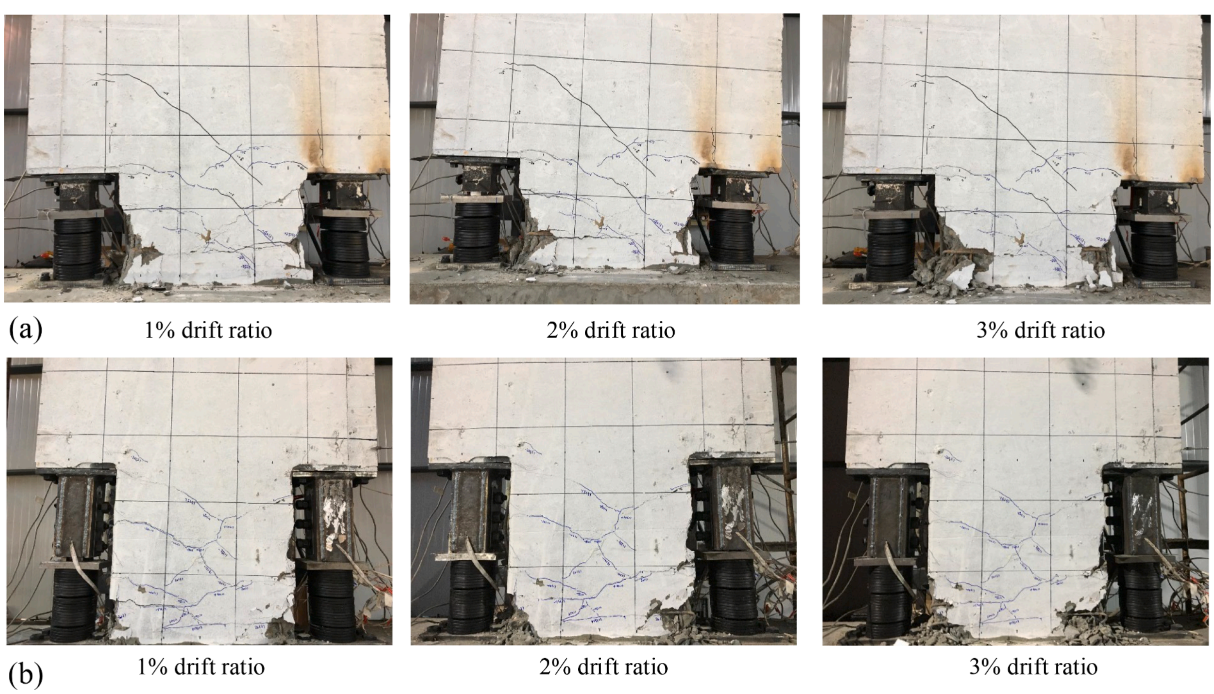

Fig. 8. The crack distributions of the test specimens at different drift ratios: (a) W1 and (b) W2.

crushing and reinforcement buckling were also observed during the test, i.e., the effects of the height, and additional friction of the DS device on the damage of the self-centering shear wall were slight. More importantly, the number of cracks of W2 was greater than that of W1, and its damage zone was slightly wider than that of W1; this was mainly due to the larger vertical deformation of the DS device of W2 during the test.

In addition, the maximum crack width of the test specimens was measured at each load–displacement amplitude, and the maximum residual crack width was also measured after unloading at each displacement amplitude to further evaluate the damage. The variations of the maximum crack width and maximum residual crack width with the displacement of the specimens are exhibited in Figs. 9 and 10, respectively. The results indicate that the maximum crack widths of the novel self-centering shear walls in stage II increased with the increase of the drift ratio, and their values were obviously greater than those in stage I. However, the maximum residual crack widths of the novel self-centering shear walls in stage II slowly increased with the increase of the drift ratio; this was mainly due to the good self-centering capability of the DS devices. The maximum crack widths of W1 and W2 in stage II were respectively 2.2 and 1.7 mm, thus reflecting respective increases of 17.4% and 11.8% as compared to those in stage I. Similarly, the maximum residual crack widths of W1 and W2 in stage II were respectively 0.18 and 0.19 mm, thus reflecting respective increases of 11.1% and 5.3% as compared to those in stage I.

Therefore, the two novel self-centering shear walls were severely damaged during the post-earthquake tests. Repair methods were thus considered to be required to maintain the normal operation of the structure after a major earthquake and aftershocks.

3.3. Hysteresis behavior

Fig. 11 presents the lateral force–displacement hysteresis curves of the test specimens. The two novel self-centering shear walls exhibited stable and repeatable hysteresis responses during the post-earthquake tests. Compared to that of the conventional shear wall, the shapes of the hysteresis curves of the self-centering shear walls were different; they exhibited flag-liked hysteresis loops, and their residual displacements were then effectively controlled. More importantly, no sudden drop in the lateral bearing capacity of the self-centering shear walls was observed during the cyclic tests in stage II, indicating that the local damage of the wall panel had no obvious impact on the ultimate bearing capacity of the whole specimen. Because additional friction of the replaceable DS devices of W2 was applied in stage II, the hysteresis loop of W2 was fuller than that of W1.

Fig. 12 further compares the backbone curves of the test specimens. It can be seen that the lateral force of W1 and W2 gradually increased with the increase of the loading displacement. The lateral force of W1 in stage II was less than that in stage I when the drift ratio was less than 1.8%, and the maximum reduction of the bearing capacity was about

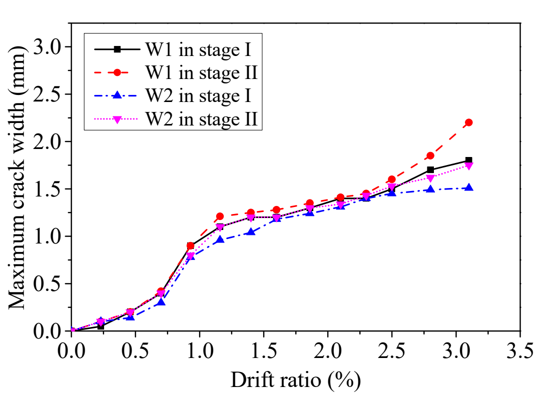

Fig. 9. The variation of the maximum crack width with displacement.

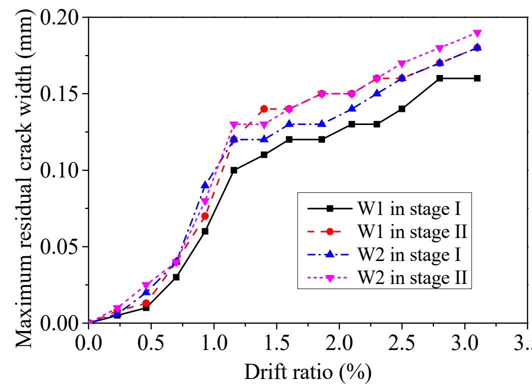

Fig. 10. The variation of the maximum residual crack width with displacement.

33.5%. When the drift ratio was greater than 1.8%, the lateral force of W1 in stage II increased to be similar to that in stage I. Similarly, the bearing capacity of W2 in stage II was less than that in stage I when the drift ratio was less than 1.4%, and its maximum reduction was about 21.8%. When the drift ratio was greater than 1.4%, the bearing capacity of W2 in stage II increased to be greater than that in stage I; it increased by 22.7% at a 3% drift ratio. The initial stiffness values K_1 (which correspond to the elastic loading stiffness and were calculated according to the backbone curves, as shown in Fig. 12) of W1 and W2 in stage II were respectively 22.52 and 30.91 kN/mm, thus reflecting respective reductions of 28.8% and 20.2% as compared to those in stage I. This is because the lateral stiffness of the specimens in stage I was applied by both the RC wall and the DS devices, while the damage was observed at the bottom RC wall of the two specimens after the test in stage I. The lateral stiffness of the specimens in stage II was mainly applied by the DS devices, thereby resulting in the reduction of the initial stiffness of the novel self-centering shear wall in stage II. The post-yield stiffness values K_2 (which correspond to the loading stiffness after the DS devices were activated and were calculated according to the hysteresis curves, as shown in Fig. 11) of W1 and W2 in stage II were respectively 1.31 and 1.04 kN/mm, which were similar to those in stage I. In addition, the loading lateral stiffnesses of W1 and W2 in stage II were stable without reduction, as exhibited in Fig. 11. This indicates that the stiffness degradation of W1 and W2 in stage II did not occur, which is helpful for improving the post-earthquake performance of the structure.

Therefore, it can be concluded that the severe local damage of the self-centering shear wall during the test in stage I only affected the initial stiffness and bearing capacity of the specimen at lower drift ratios. The post-yield stiffness and ultimate bearing capacity can be steadily provided by the replaceable DS devices, and the bearing capacity can be effectively increased by increasing their friction. As a result, the temporary operation of the self-centering shear wall after an earthquake can be assured, which is helpful for emergency services and disaster relief, i.e., the bearing capacity of the self-centering shear wall is satisfactory.

3.4. Post-earthquake performance evaluation

The energy dissipation capability, the residual displacement, and the strain distribution, which can reflect the seismic behavior of the self-centering shear wall, were calculated and analyzed based on the test results of stage II. Fig. 13 presents the comparison of the cumulative energy dissipation (which was calculated by the sum of the area of the hysteresis loop at each loading displacement amplitude) of the test specimens. The cumulative energy dissipation of the two self-centering shear walls in stage II was found to gradually increase with the increase of the displacement, and that of W1 in stage II was relatively lower than that in stage I at the same drift ratio, as shown in Fig. 13(a). This was due to the local damage of the RC wall during the test in stage I,

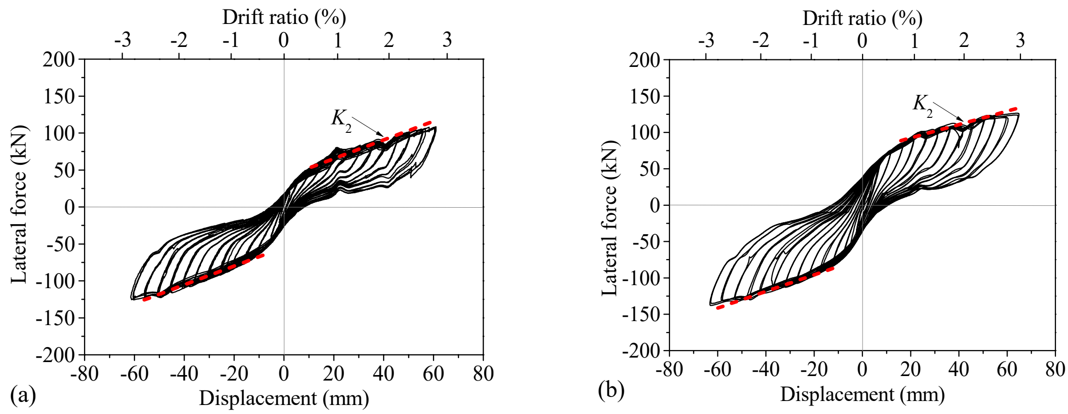

Fig. 11. The hysteresis curves of the test specimens: (a) W1 and (b) W2.

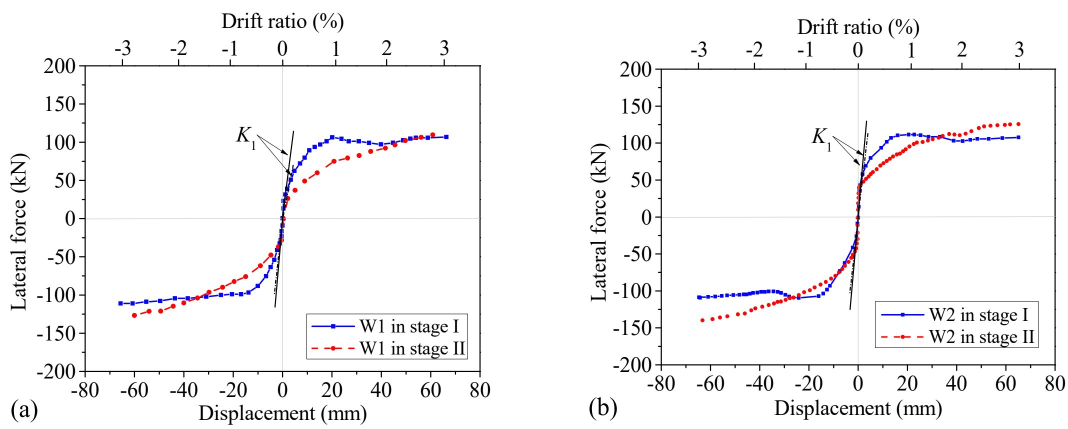

Fig. 12. The comparison of the backbone curves of the test specimens: (a) W1 and (b) W2.

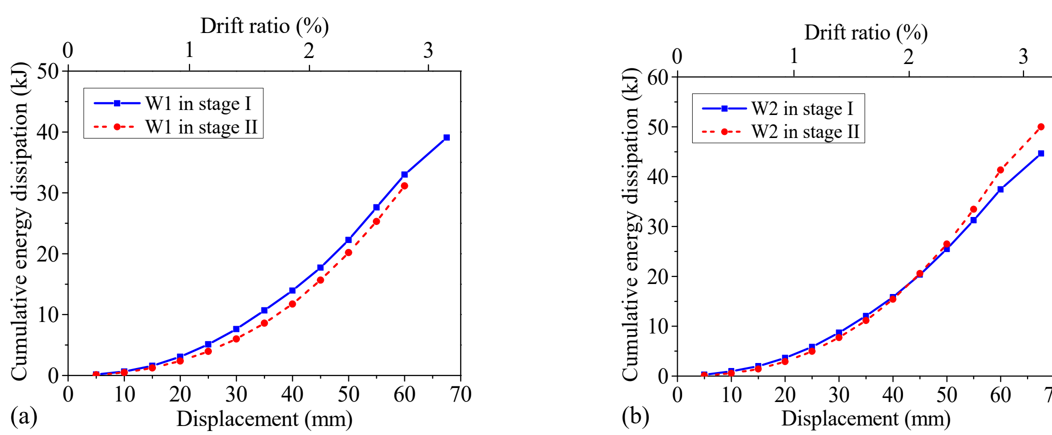

Fig. 13. The comparison of the energy dissipation of the specimens: (a) W1 and (b) W2.

i.e., the energy dissipation capability of the self-centering shear wall was slightly reduced after the earthquake. When increasing the friction of the replaceable devices, the cumulative energy dissipation of W2 correspondingly increased with the increase of the loading displacement; when the drift ratio reached 3%, the cumulative energy dissipation of W2 in stage II increased by 16.8% as compared to that in stage I. These results indicate that although local severe damage of the self-centering shear wall will occur during an earthquake, it still can effectively dissipate energy without repair; thus, the normal operation of the structure after an earthquake can be maintained.

The residual displacement was obtained based on the hysteresis loop at the first cycle of each loading step, and the value was taken as the mean value of the positive and negative residual displacements. The residual displacements of the specimens during the test in stage II are presented in Fig. 14, in which the residual displacements of the conventional wall [21], W1 in stage I [21], and W2 in stage I [22] were also compared. It was found that the residual displacements of W1 and W2 gradually increased with the increase of the loading displacement, and the rate of W2 was faster than that of W1 due to the additional friction. However, the residual drift ratios of W1 and W2 in stage II were correspondingly lower than that of the conventional wall, as shown in Fig. 14. When the drift ratio reached 2.1%, the residual drift ratio of the

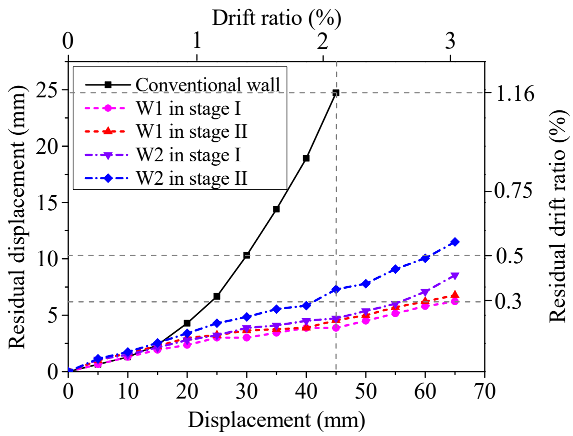

Fig. 14. The residual displacement of the specimens during the test in stage II.

conventional wall was 1.16% with severe damage, and it would be difficult to repair; in contrast, the residual drift ratios of W1 and W2 in stage II were respectively 0.21% and 0.34%, thus reflecting respective reductions of 81.9% and 70.7%. It should be noted that the residual displacements of W1 and W2 in stage II were larger than those in stage I due to the damage accumulation in the first test. As shown in Fig. 14, the maximum residual drift ratios of W1 and W2 in stage II were respectively 0.32% and 0.53%, thus reflecting respective increases of 8.1% and 25.5% as compared to those in stage I. According to the comparison results of W2 in stage I and stage II, the residual drift ratio increased due to the increase of the friction of the DS devices. However, the maximum residual drift ratio of W1 was still less than 0.5%, and that of W2 was just over 0.5%. This indicates that the self-centering capability of the specimens after several earthquakes was still satisfactory, so structures with self-centering shear walls are necessary and valuable for repair.

To determine the inner damage state of the self-centering shear wall in stage II, the strain distribution at key positions was analyzed. The strain distributions of the concrete and steel reinforcements of W1 and W2 in stage II are presented in Fig. 15. Because local damage was observed at the bottom corners of the self-centering shear wall in stage I, the bottom strain gauges were invalid; thus, the strain of the concrete at the height of 500 mm (Fig. 15(a)) of the self-centering shear wall was monitored during the post-earthquake test. It can been seen that the maximum concrete strains of W1 and W2 were under compression, and their maximum values were respectively 0.00027 and 0.0004. This result indicates that the concrete strains at the height of 500 mm of the self-centering shear walls were far less than the peak strain of concrete; thus, the upper part of the RC wall was considered to be intact.

Because the deformation and damage were concentrated at the lower part of the self-centering shear wall, the strains of the longitudinal reinforcement, the horizontal reinforcement, and the stirrup at the bottom zone (Fig. 15(b), (c), and (d), respectively) of the RC wall were respectively investigated. The strains of the longitudinal reinforcements of the specimens were relatively large; as shown in Fig. 15(b), the maximum values of W1 and W2 were respectively 0.0016 and 0.0012, which were still less than the yield strain of the steel bar with a value of 0.0021. However, the strain of the longitudinal reinforcement at the edge of the RC wall was large, and the values during the post-earthquake test were not obtained due to the invalid strain gauges. The strains of the horizontal reinforcement and stirrup of W1 and W2 were less, indicating the good shear capacity of the self-centering shear wall. Therefore, it can

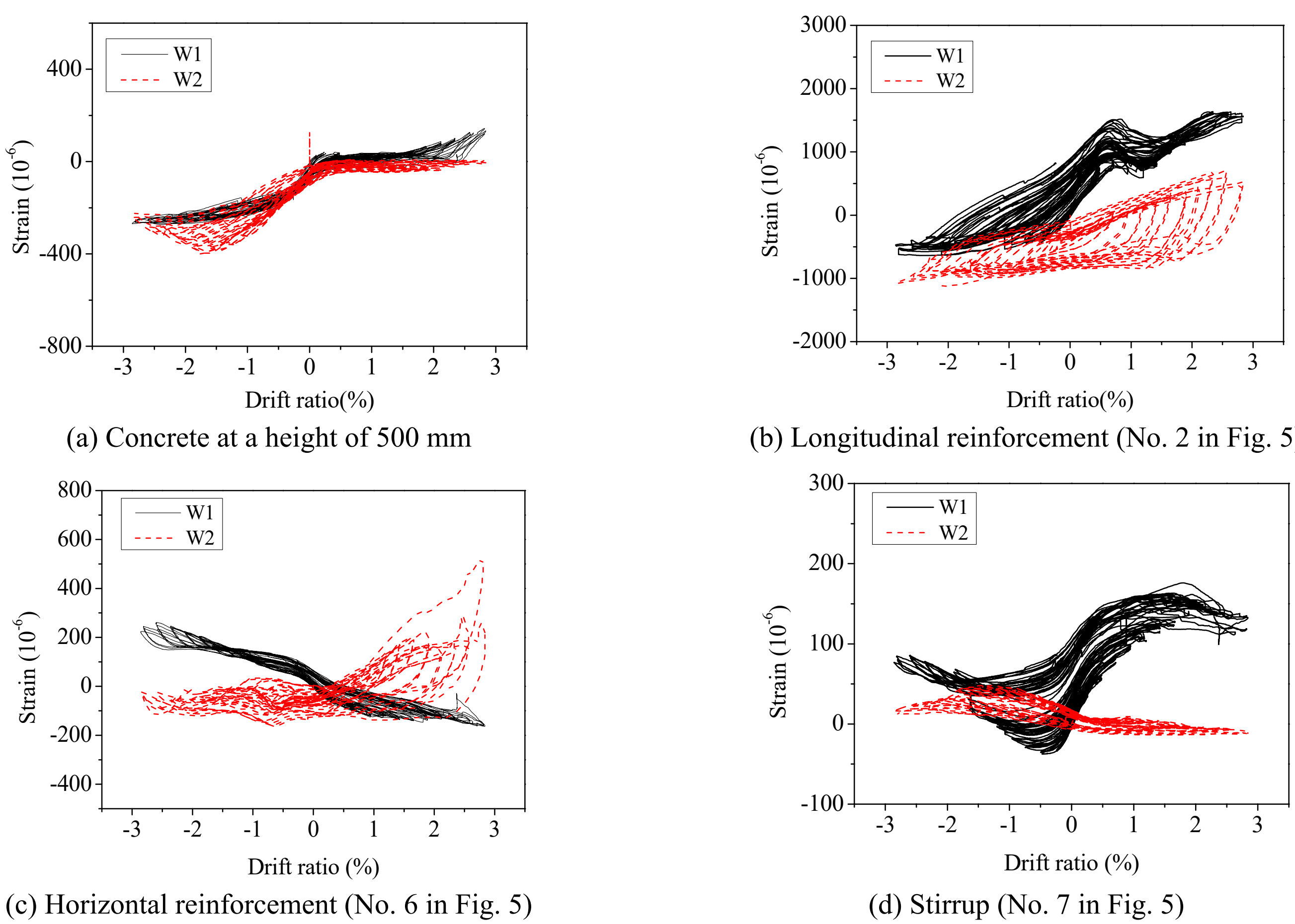

Fig. 15. The strain distributions of the concrete and steel reinforcements of W1 and W2 in stage II.

be concluded that the severe damage of the self-centering shear wall during the post-earthquake test was mainly concentrated at the bottom corners, while the other parts were only slightly damaged or remained intact. Thus, the damaged zone of the specimen would need to be repaired after several earthquakes to restore the normal function of the structure.

Additionally, the damage of the replaceable DS devices of the test specimens was evaluated via the strain records of the outer tubes, as shown in Fig. 6. The strains of the replaceable DS devices of both W1 and W2 in stage II were correspondingly larger than those in stage I; this was mainly due to the more severe damage of the RC wall panel in stage II, which resulted in larger deformation at the bottom of the specimens. The maximum strains of W1 and W2 in stage II were 0.00111 and 0.0005, respectively, which were still far less than the yield strain of the steel. Thus, the replaceable DS devices of W1 and W2 were considered to have remained intact after being subjected to the two cyclic loading tests.

4. Improvement methods

4.1. Reinforcement of the RC wall

Because the damage of the novel self-centering shear wall was mainly concentrated at the corner of the RC wall and its residual deformation after two cyclic loading tests was acceptable, the repair of the RC wall after being subjected to a major earthquake and aftershocks was considered to be effective and economical. Therefore, a method for the reinforcement of the novel self-centering shear wall is proposed, as shown in Fig. 16. The reinforcement of the novel self-centering shear wall after an earthquake is mainly divided into four steps. First, the original concrete at the damage zone of the RC wall panel must be cleaned, and the longitudinal reinforcements, horizontal reinforcements, and stirrups must then be locally exposed, as shown in Fig. 16(a). Second, the yielded and buckled longitudinal reinforcements at the exposed zone of the RC wall must be cut off, and the local concrete of the foundation must also be cleaned to expose the local longitudinal reinforcements embedded in the foundation. Then, the replaceable longitudinal reinforcements must be welded with the original longitudinal reinforcements embedded in the concrete. In addition, the damaged stirrups must also be replaced. Third, after the repair of the steel reinforcement cage, the concrete at the damage zone must be cast and cured again (Fig. 16(b)). Finally, a glass fiber-reinforced polymer (GFRP) sheet was attached at the bottom part of the wall panel to strengthen its bearing capacity and initial stiffness, as shown in Fig. 16 (c). It should be noted that the angled edge of the square wall panel should be polished before wrapping the GFRP sheets.

According to a previous study on GFRP sheet confined square specimens [25–29], reinforcement via the GFRP sheet was useful for improving the bearing capacity and stiffness of the specimens. Therefore, after a major earthquake and aftershocks, the function of the novel self-centering shear wall can be quickly restored with the proposed repair method. Additionally, the novel self-centering shear wall can also be strengthened at its initial state with GFRP sheets to reduce the corner damage and improve the post-earthquake performance.

4.2. Improved configuration of the self-centering shear wall

On the other hand, the severe damage of the concrete was also due to its poor tensile capacity; because the RC wall panel of the novel self-centering shear wall was fixed on the foundation, the tensile deformation at the bottom of the specimen was relatively large, resulting in the failure of the concrete. Therefore, the configuration of the self-centering shear wall was improved to avoid the severe damage of the RC wall, as shown in Fig. 17. The constraint between the RC wall and the foundation was relaxed. As shown in Fig. 17, the RC wall was connected to the foundation through two self-centering DS devices and two friction energy dissipation devices, and only high-strength bolts were used for the assembly of the improved self-centering shear wall.

The main parts of the self-centering DS device in the improved self-centering shear wall were similar to those of the previous novel self-centering shear wall, as shown in Fig. 18. They consisted of DSs, an inner tube, an outer tube, DS plates, and lower and upper connecting plates. The difference is that the self-centering DS device exhibited a symmetrical force–displacement curve under compression and tension, as shown in Fig. 18. Therefore, the self-centering DS device can effectively provide a larger restoring force for the whole specimen when subjected to cyclic loading. More importantly, the residual deformation of the self-centering DS device can be basically eliminated, which can help to restore the wall specimen to its initial state during an earthquake.

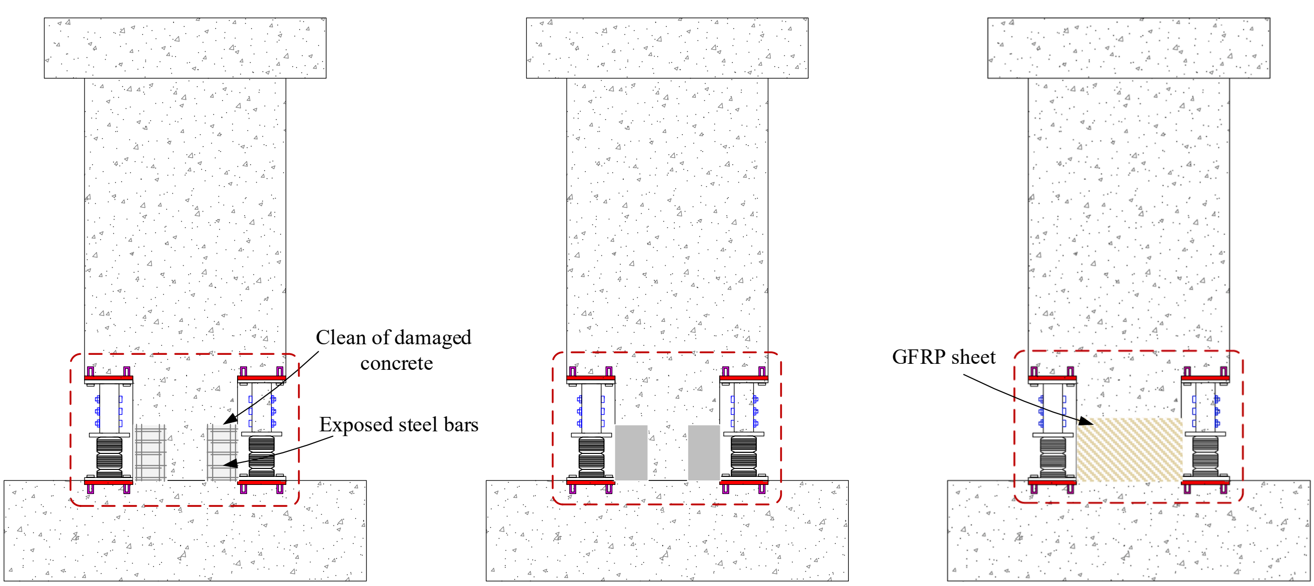

(a) Concrete clean and steel bar replacement of the damaged zone
(b) Concrete pouring
(c) GFRP wrapping

Fig. 16. The process of the reinforcement of the novel self-centering shear wall.

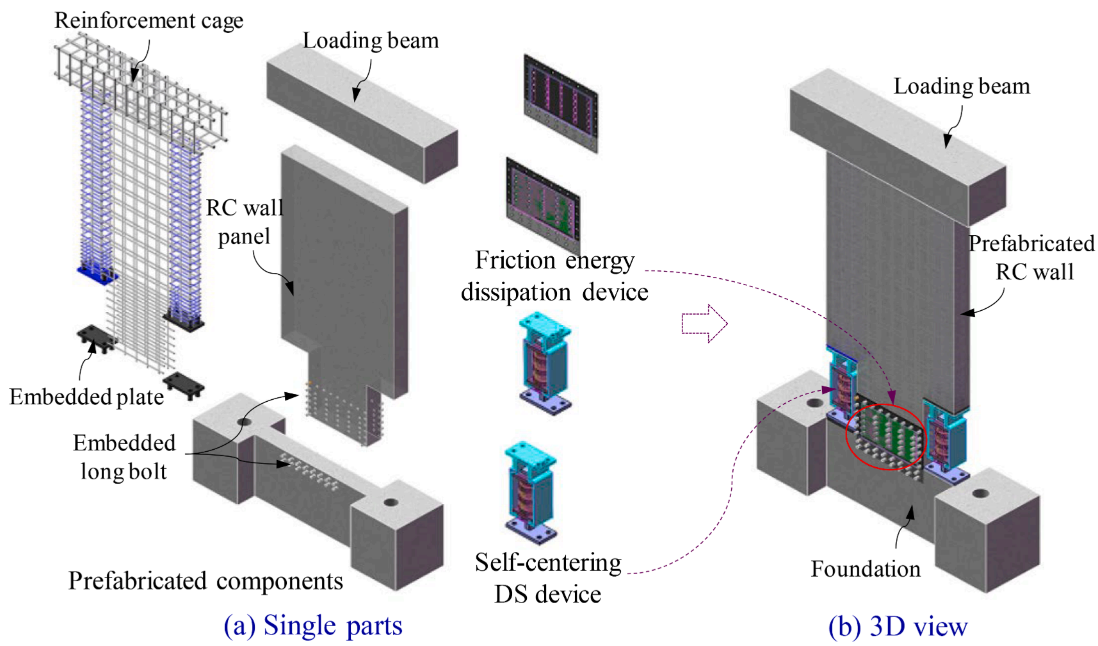

Fig. 17. The configuration of the improved self-centering shear wall.

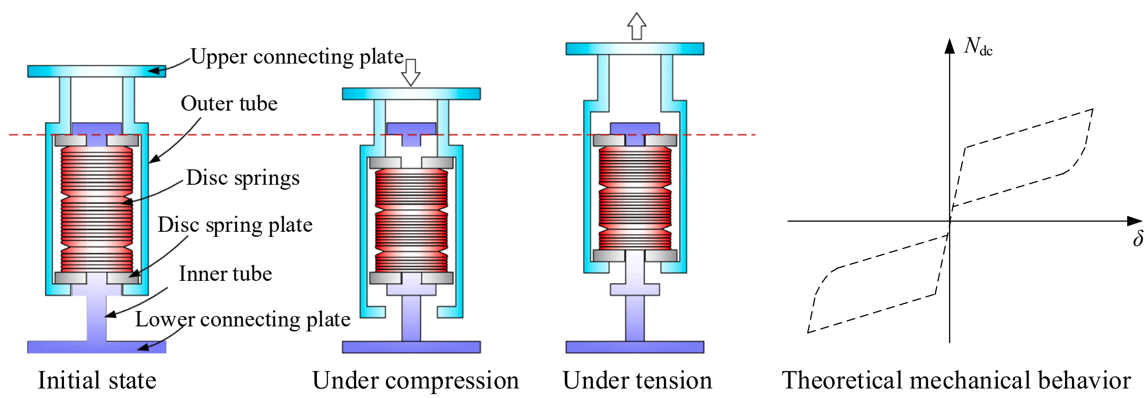

Fig. 18. The configuration and mechanics of the self-centering DS device.

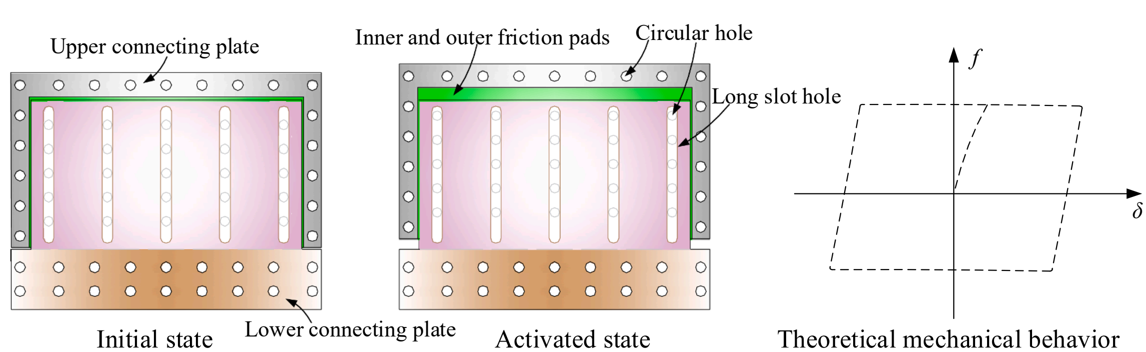

Fig. 19. The configuration and mechanics of the friction energy dissipation device.

The configuration of the friction energy dissipation device is shown in Fig. 19. The upper and lower connecting plates were respectively fixed on the RC wall and foundation with high-strength bolts. An inner friction pad was placed on the upper connecting plate, and circular holes were set in them. An outer friction pad was placed on the lower connecting plate, and long slot holes were set in them. The wall panel was connected to the foundation with high-strength bolts in the friction pad area, and the friction was also applied by these bolts. The friction energy dissipation device exhibited full energy dissipation capability, as shown in Fig. 19. Therefore, the friction energy dissipation device can effectively dissipate energy when subjected to strong earthquakes. More importantly, the RC wall panel rocks after the activation of the friction energy dissipation devices, thus addressing the damage of the concrete at the wall corners due to tensile force. Thus, the post-earthquake performance of the improved self-centering shear wall can be greatly improved, and it is expected to operate normally without repair after an earthquake.

To predict the hysteresis behavior of the improved self-centering shear wall, a numerical method was proposed. Fig. 20 presents the numerical model of the improved self-centering shear wall, the modeling was conducted in OpenSees software. The RC wall panel was modeled by the ShellMITC4 element, which is a four-node plane stress quad element with eight degrees of freedom. The longitudinal reinforcements of the boundary zones were modeled by the fiber elements. The self-centering DS device and friction energy dissipation device was modeled by the truss element. The material properties of the RC wall panel and steel bars have been introduced in reference [30]. The theoretical behaviors of the self-centering DS device and friction energy dissipation device were modeled by the SelfCentering material and Steel02 material, respectively, as shown in Fig. 20(d) and (e). Because the RC wall was connected to the foundation through the friction energy dissipation device, it can only sustain compression. Thus, zero-lenth elements were used between the foundation nodes and bottom wall nodes (Fig. 20), and only compressed and tension-free material (Fig. 20(f)) was applied to these zero-lenth elements to model the behavior of the interface between the RC wall and foundation.

The geometric sizes and material properties of the RC wall were same with those of W2, the parameters including the initial stiffness K_{ini}, post-activation stiffness K_d, activation force F_y, and α of the self-centering DS device were determined based on those of the DS device of W2. The values of K_{ini}, K_d, F_y, and α of the self-centering DS device were 182.3 kN/mm, 5.5 kN/mm, 100 kN/mm, and 1.0, respectively. The friction force N_f of the friction energy dissipation device was calculated based on the yield strength of the distributed longitudinal reinforcements, and its value was 45 kN. Fig. 21 shows the hysteresis curve of the improved self-centering shear wall. It can be seen that the improved self-centering shear wall exhibited flag-shaped hysteresis response. The bearing

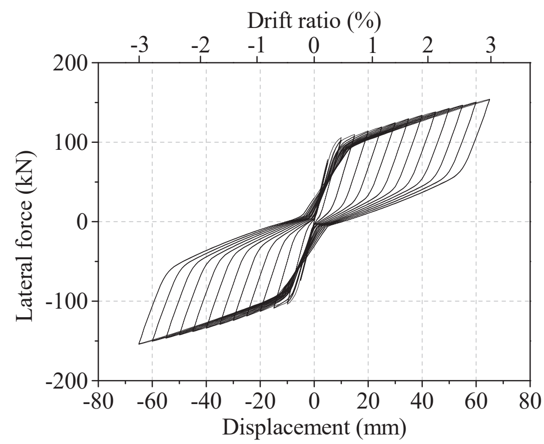

Fig. 21. Hysteresis curve of the improved self-centering shear wall.

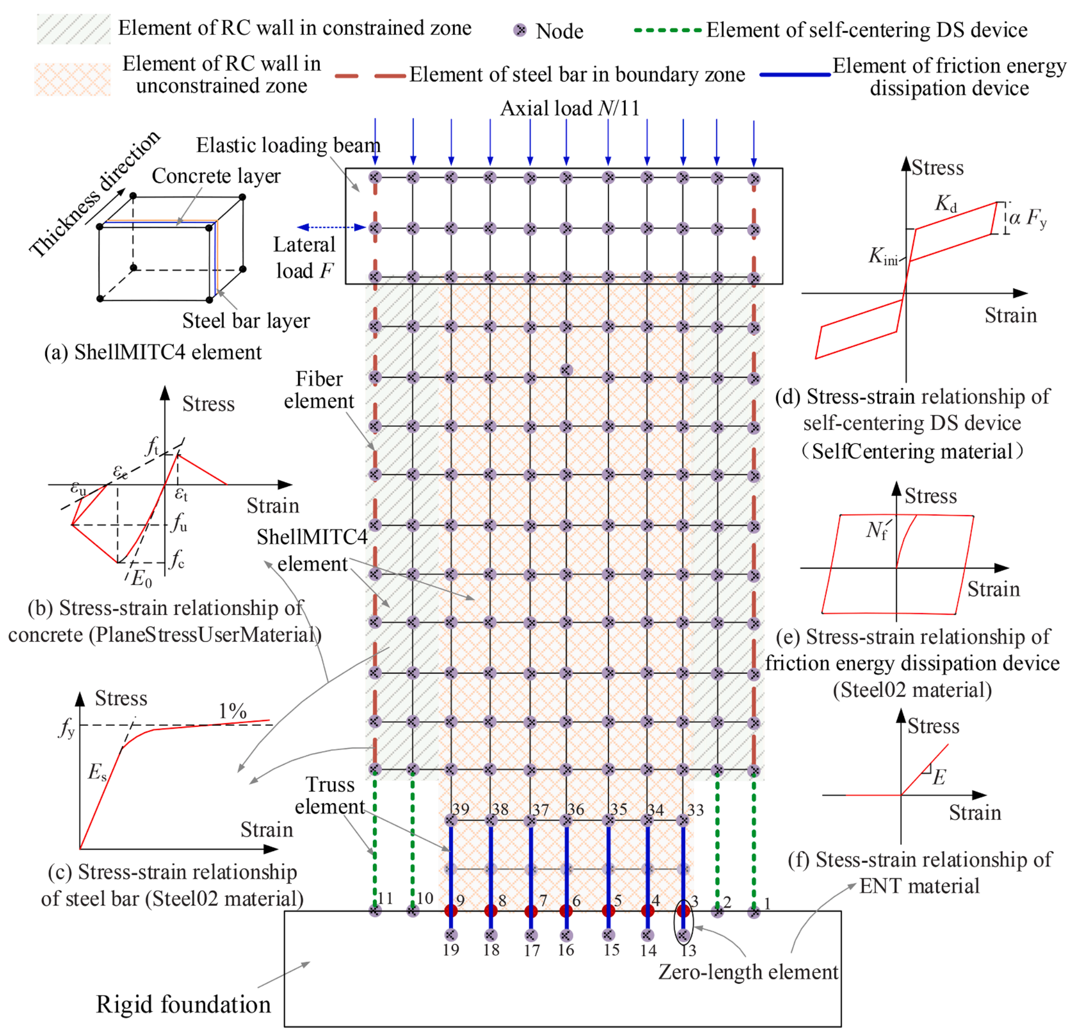

Fig. 20. Numerical model of the improved self-centering shear wall.

capacity gradually increased with the increase of the displacement, and the hysteresis loop is relatively full, indicating it has good energy dissipation capability. Additionally, the residual displacement of the improved self-centering shear wall was significantly reduced, indicating that the self-centering DS device can effectively restore the RC wall to the position before loading. When the drift ratio reached 3%, no decrease of the bearing capacity and loading stiffness of the inproved self-centering shear wall was observed. This indicates that the energy was mainly dissipated by the self-centering DS device and friction enery dissipation device, and no severe damage will accumulated in the RC wall. Therefore, the satisfactory seismic resilience of the improved self-centering shear wall was preliminarily verified by the numerical results.

5. Conclusions

The damage of a novel self-centering shear wall with replaceable DS devices subjected to cyclic loading was investigated to evaluate its normal operation ability after an earthquake. Cyclic loading tests were directly conducted on two damaged self-centering shear walls to evaluate their post-earthquake performance. The following conclusions were drawn from this research.

(1) Obvious local concrete spalling at the bottom corners of the novel self-centering shear walls was observed at a 2.1% drift ratio during the first cyclic loading test, but the steel bar was not exposed. Moreover, the maximum strains of the concrete, reinforcements, and DS devices were less than their peak values. Therefore, the novel self-centering shear wall specimens were considered fit for further testing to investigate their post-earthquake performance.
(2) The novel self-centering shear walls exhibited stable flag-liked hysteresis behavior during the post-earthquake tests. The bearing capacities of the two specimens under the second loadings decreased at smaller drift ratios as compared to those under the first loadings, and the maximum reductions were about 33.5% and 21.8%, respectively. However, no decrease of the ultimate bearing capacity of the specimens occurred, and it could be effectively increased by increasing the friction of the replaceable DS devices. In addition, the energy dissipation capabilities of the novel specimens in the first and second loadings were similar, and the residual drift ratios of the two novel specimens after the second loadings were still less than 0.5% at a 2.1% drift ratio. Therefore, the post-earthquake performance of the novel self-centering shear wall was satisfactory.
(3) The damage at the bottom corners of the novel self-centering shear walls became more severe during the post-earthquake tests with obvious concrete crush and reinforcement buckling. In contrast, the maximum strains of the concrete, reinforcements, and DS devices at the upper parts were acceptable. Thus, after being subjected to several earthquakes, the repair of the damage zone of the novel self-centering shear wall would be needed to maintain the normal operation of the structure.
(4) To improve the post-earthquake performance of the novel self-centering shear wall, two reinforcement methods were proposed. Due to the good self-centering capability of the novel self-centering shear wall, its damage zone can be easily strengthened via GFRP sheets to restore its normal function after earthquakes. Moreover, an improved configuration between the RC wall and the foundation was developed to reduce the damage of the novel self-centering shear wall, thereby avoiding its repair after earthquakes. The numerical result indicates that improved self-centering shear wall exhibited flag-shaped hysteresis response with good energy dissipation and self-centering capabilities, and no severe damage will accumuated in the RC wall. Therefore, the satisfactory seismic resilience of the improved self-centering shear wall was preliminarily verified.

This study was focused on the post-earthquake performance of a single self-centering shear wall, and the influence of its design on the seismic resilience of the whole structure with different components is not clear. Therefore, the seismic resilience of a structure with a\self-centering shear walls will be particularly investigated in the future.

CRediT authorship contribution statement

Shuijing Xiao: Methodology, Investigation, Data curation, Writing – review & editing. **Longhe Xu:** Conceptualization, Methodology, Supervision, Project administration, Writing – review & editing. **Peng Feng:** Conceptualization, Methodology, Supervision, Project administration, Writing – review & editing.

Declaration of Competing Interest

The authors declare that they have no known competing financial interests or personal relationships that could have appeared to influence the work reported in this paper.

Data availability

Data will be made available on request.

Acknowledgments

The writers gratefully acknowledge the partial support of this research by the National Natural Science Foundation of China (No. 52208263 and No. 52125804) and the China Postdoctoral Science Foundation Grant (No. 2022M711867).

References

[1] Perez FJ, Sause R, Pessiki S. Analytical and experimental lateral load behavior of unbonded posttensioned precast concrete walls. J Struct Eng 2007;133(11):1531–40.
[2] Lu XL, Mao YJ, Chen Y, Liu JJ, Zhou Y. New structural system for earthquake resilient design. J Earthq Tsunami 2013;7(3):1350013.
[3] Garmeh V, Akbarpour A, Adibramezani M, Kashani AH, Adibi M. SMA-based self-centering eccentrically braced frame with vertical link member. Structures 2022;43:1230–58.
[4] Yam MCH, Ke K, Huang Y, Zhou XH, Liu YC. A study of hybrid self-centring beam-to-beam connections equipped with shape-memory-alloy-plates and washers. J Constr Steel Res 2022;198:107526.
[5] Hu SL, Wang W, Alam MS. Hybrid self-centering rocking core system with fiction spring and viscous dampers for seismic resilience. Eng Struct 2022;257:114102.
[6] Xu LH, Lin ZC, Xie XS. Assembled self-centering energy dissipation braces and a force method-based model. J Constr Steel Res 2022;190:107121.
[7] Zhang Y, Xu LH. Cyclic response of a self-centering RC wall with tension-compression-coupled disc spring devices. Eng Struct 2022;250:113404.
[8] Holden T, Restrepo J, Mander JB. Seismic performance of precast reinforced and prestressed concrete walls. J Struct Eng 2003;129(3):286–96.
[9] Henry RS, Sritharan S, Ingham JM. Finite element analysis of the PreWEC self-centering concrete wall system. Eng Struct 2016;115:28–41.
[10] Guo T, Wang L, Xu ZK, Hao YW. Experimental and numerical investigation of jointed self-centering concrete walls with friction connectors. Eng Struct 2018;161:192–206.
[11] Chen F, Li Z, He MJ, Wang YB, Shu Z, He GR. Seismic performance of self-centering steel-timber hybrid shear wall structures. J Build Eng 2021;43:102530.
[12] Lu XL, Dang XL, Qian J, Zhou Y, Jiang HJ. Experimental study of self-centering shear walls with horizontal bottom slits. J Struct Eng 2017;143(3):04016183.
[13] Kurama YC, Weldon BD, Shen Q. Experimental evaluation of posttensioned hybrid coupled wall subassemblages. J Struct Eng 2006;132(7):1017–29.
[14] Kurama YC, Shen Q. Posttensioned hybrid coupled walls under lateral loads. J Struct Eng 2004;130(2):297–309.
[15] Sritharan S, Aaleti S, Henry RS, Liu KY, Tsai KC. Precast concrete wall with end columns (PreWEC) for earthquake resistant design. Earthq Eng Struct D 2015;44(12):2075–92.
[16] Huang XG, Wang YH. Development and modelling of new friction damped self-centring link for coupled wall systems. Eng Struct 2021;239:112365.
[17] Lu JY, Zhang HY, Yu SJ. Study on seismic behaviors of self-centering steel plate shear walls with slits. J Constr Steel Res 2021;185:106878.
[18] Restrepo JI, Rahman A. Seismic performance of self-centering structural walls incorporating energy dissipators. J Struct Eng 2007;133(11):1560–70.
[19] Zhang Y, Xu LH. Experimental investigation of a new self-centering shear wall with resilient hinge devices. Eng Struct 2022;266:114657.

[20] Zhai ZP, Guo W, Liu YH, Ma YH, Zhou FL. New precast self-centering rocking shear wall with multiple hinged joints: description and design approach for seismic protection of buildings. Eng Struct 2022;262:114401.
[21] Xiao SJ, Xu LH, Li ZX. Development and experimental verification of self-centering shear walls with disc spring devices. Eng Struct 2020;213:110622.
[22] Xu LH, Xiao SJ, Li ZX. Experimental investigation on seismic behavior of a new self-centering shear wall with additional friction. J Struct Eng 2021;147(5):04021056.
[23] GB 50011-2010. Code for seismic design of buildings. Beijing: Ministry of Housing and Urban-Rural Development of the People's Republic of China; 2010.
[24] Xu LH, Xiao SJ, Li ZX. Hysteretic behavior and parametric studies of a self-centering RC wall with disc spring devices. Soil Dyn Earthq Eng 2018;115:476–88.
[25] Chen ZP, Song CM, Li SX, Zhou J. Flexural bearing capacity and stiffness research on CFRP sheet strengthened existing reinforced concrete poles with corroded connectors. Struct Monit Mainten 2022;9(1):29–42.
[26] Deng KL, Pan P, Shen SD, Wang HS, Feng P. Experimental study of FRP-reinforced slotted RC shear walls under cyclic loading. J Compos Constr 2018;22(4):04018017.
[27] Feng P, Cheng S, Bai Y, Ye L. Mechanical behavior ofconcrete-filled square steel tube with FRP-confined concrete core sub-jected to axial compression. Compos Struct 2015;123(5):312–24.
[28] Wang ZY, Li ZY, Yang JQ, Huang FS, Feng P. Axial compressive and seismic performance of GFRP wrapped square RC columns with different scales. J Build Eng 2022;62:105342.
[29] Leal-Graciano JM, Quiñónez B, Rodríguez-Lozoya HE, Pérez-Gavilán JJ, Lizárraga-Pereda JF. Use of GFRP as retrofit alternative for confined masonry walls with window opening subjected to in-plane lateral load. Eng Struct 2020;223:111148.
[30] Xu LH, Xiao SJ, Li ZX. Behaviors and modeling of new self-centering RC wall with improved disc spring devices. J Eng Mech 2020;146(9):04020102.